Progress in Biophysics and Molecular Biology 149 (2019) 39–53

Contents lists available at ScienceDirect

Progress in Biophysics and Molecular Biology

journal homepage: www.elsevier.com/locate/pbiomolbio

From non-excitable single-cell to multicellular bioelectrical states supported by ion channels and gap junction proteins: Electrical potentials as distributed controllers

Javier Cervera [a, *], Vaibhav P. Pai [b], Michael Levin [b], Salvador Mafe [a]

[a] Dept. Termodinàmica, Universitat de València, E-46100, Burjassot, Spain
[b] Dept. of Biology and Allen Discovery Center at Tufts University, Medford, MA, 02155-4243, USA

ARTICLE INFO

Article history:
Received 24 April 2019
Accepted 26 June 2019
Available online 27 June 2019

Keywords:
ion channels
Bioelectrical memory
Multicellular electrical patterns
Spatially distributed controller
Embryogenesis
Tumorigenesis

ABSTRACT

Endogenous bioelectric patterns within tissues are an important driver of morphogenesis and a tractable component of a number of disease states. Developing system-level understanding of the dynamics by which non-neural bioelectric circuits regulate complex downstream cascades is a key step towards both, an evolutionary understanding of ion channel genes, and novel strategies in regenerative medicine. An important capability gap is deriving rational modulation strategies targeting individual cells' bioelectric states to achieve global (tissue- or organ-level) outcomes. Here, we develop an ion channel-based model that describes multicellular states on the basis of spatio-temporal patterns of electrical potentials in aggregates of non-excitable cells. The model is of biological interest because modern techniques allow to associate bioelectrical signals with specific ion channel proteins in the cell membrane that are central to embryogenesis, regeneration, and tumorigenesis. As a complementary approach to the usual biochemical description, we have studied four biophysical questions: (*i*) how can single-cell bioelectrical states be established; (*ii*) how can a change in the cell potential caused by a transient perturbation of the cell state be maintained after the stimulus is gone (bioelectrical memory); (*iii*) how can a single-cell contribute to the control of multicellular ensembles based on the spatio-temporal pattern of electrical potentials; and (*iv*) how can oscillatory patterns arise from the single-cell bioelectrical dynamics. Experimentally, endogenous bioelectric gradients have emerged as instructive agents for morphogenetic processes. In this context, the simulations can guide new procedures that may allow a *distributed control* of the multicellular ensemble.

1. Introduction

Advances in regenerative medicine require rational control over the processes that enable cells to coordinate their activities toward the construction and repair of complex anatomies. An important component of this research program is the computational modeling of the communication and signaling pathways that occur during in vivo morphogenesis. This is essential, in order to enable workers in regenerative medicine and synthetic bioengineering to identify efficient control knobs: transient, localized interventions that trigger predictable and complex system-level changes that propagate across tissue distance and continue long after the stimulus has been discontinued (Chernet and Levin, 2014; Herrera-Rincon et al., 2018).

There are different layers of description for intra and intercellular communication that concern molecular-genetic, reaction-diffusion, biomechanical, and bioelectrical processes interconnected by complex feedbacks. The results to be presented here concern the *bioelectrical* layer for both *single-cell* and *multicellular* processes. In the case of *non-excitable* (non-neural) cells, this layer is usually disregarded in favor of the molecular-genetic and reaction-diffusion layers. For instance, theoretical proposals concerning biological computation with proteins tend to focus on single-cell biochemical concepts and networks, thus neglecting significant bioelectrical processes regulated by the ion channel proteins in the cell membrane (Hille, 1992; Kirkton and Bursac, 2011). Experimentally, multicellular processes and cell bioelectricity are central to embryogenesis, regeneration, and

* Corresponding author.
E-mail address: javier.cervera@uv.es (J. Cervera).

https://doi.org/10.1016/j.pbiomolbio.2019.06.004
0079-6107/

tumorigenesis (Soto and Sonnenschein, 2011; Yang and Brackenbury, 2013; Pai et al., 2015; Levin et al., 2017; Busse et al., 2018). Although transcription factors depend on specific molecules and biochemical pathways, the fact is that bioelectrical magnitudes such as cell membrane potentials can indirectly modulate transcription by influencing the local concentration of these molecules and crucial biochemical steps (Cervera et al., 2016, 2018a).

The experimental techniques currently available allow to link bioelectrical signals with specific ion channel proteins (Kirkton and Bursac, 2011; Yang and Brackenbury, 2013; Bates, 2015; McNamara et al., 2016; Chernet et al., 2016; Levin et al., 2017) and permit recordings from multicellular assemblies (Kirkton and Bursac, 2011; Emmons-Bell et al., 2015; Krüger and Bohrmann, 2015; Tsiairis and Aulehla, 2016; Durant et al., 2017; Pai et al., 2018; Staufer et al., 2019). Levin and co-workers (Chernet et al., 2015; Pai et al., 2015; Levin et al., 2017; Mathews and Levin, 2017; Pietak and Levin, 2017; Cervera et al., 2018a) have recently employed different procedures to modify single and multicellular states by acting on endogenous electric potential differences – no external electric field is applied (Figs. 1 and 2). For instance, the Goldman-Hodgking-Katz equation shows that single-cell potentials can be modified by changing the ionic concentrations and the ion channel permeability, which is proportional to the channel conductance (Hille, 1992).

However, most biological systems show complex feedback processes, such as physiological homeostasis or the ability of highly-abnormal tadpoles to build normal frog faces and stop remodeling when the correct frog face has been achieved (Vandenberg et al., 2012). Also, externally increasing a specific protein level does not always correlate with the expected increase in the ion channel functional activity; compensatory effects between redundant channels may also arise. In addition, ionic concentrations and ion channel conductances are interrelated: the activation potential of inwardly rectifying potassium channels (*Kir*) can be shifted to more positive potentials by increasing the extracellular K^+ concentration but this depolarization process may also be influenced by the concomitant blocking of *Kir* due to barium ions and polyamines that act to decrease the effective channel conductance (Hille, 1992). In the case of intercellular gap junctions, particular connexin proteins can show opposite actions because of conflicting channel-dependent and independent functions (Sin et al., 2012).

While the above biological complexity may suggest the need for highly specific context-dependent external actions, it is of current interest to find out if average magnitudes not requiring a microscopic subcellular management could allow the control of multicellular ensembles (Levin et al., 2017; Mathews and Levin, 2017). In chemical engineering, for instance, the macroscopic control of a few average magnitudes has proved more useful than a detailed molecular description because the basic units are either structureless (atoms in a gas, electrons in a semiconductor) or their microscopic properties emerge as a macroscopic average property (water molecules and viscosity effects in fluid mechanics). Admittedly, this approach has been difficult to pursue in the case of *single-cell* molecular biology because many structural details that escape a mean-field regulation are often relevant. However, such top-down approaches have been suggested as an essential path toward overcoming the complexity barrier that currently limits regenerative medicine advances focused on bottom-up manipulation of individual genes or factors (Pezzulo and Levin, 2016).

Figs. 1 and 2 suggest that patterns of electric potentials established over a multicellular ensemble allow a sort of *memory* that controls target biological outcomes and can be reprogrammed by appropriate goal-oriented external actions. Other biological systems showing similar experimental trends have been described with detail elsewhere (Pai et al., 2015, 2018; Levin et al., 2017; Mathews and Levin, 2017). Studying possible mechanisms for implementing memory in non-neural systems is important not only for understanding complex behavioral capacities during primitive cognition in a range of aneural organisms (Baluška and Levin, 2016), but also for implementing artificial living machines with memory functions (Kamm et al., 2018). Here, we will explore qualitative theoretical descriptions based on ion channels and bioelectrical properties such as average electric potentials in order to establish a *goal-oriented control* of non-excitable cell ensembles.

Distributed computation allows the control of synthetic biological devices (Macía et al., 2012; Cheney et al., 2015). We consider the electric potential as a *distributed controller* of target multicellular outcomes. Our rationale is based on the following facts: (*i*) the bioelectrical *single-cell state* can be *controlled* at the *ensemble level* because of the coupling with the neighboring cells; (*ii*) *spatial distributions* of electric potential can be established over different regions in a multicellular ensemble; (*iii*) the resulting spatio-temporal regionalization (*pattern*) is *instructive* for target biological outcomes allowing thus a *distributed control* of the ensemble towards specific goals; and (*iv*) these electric potential

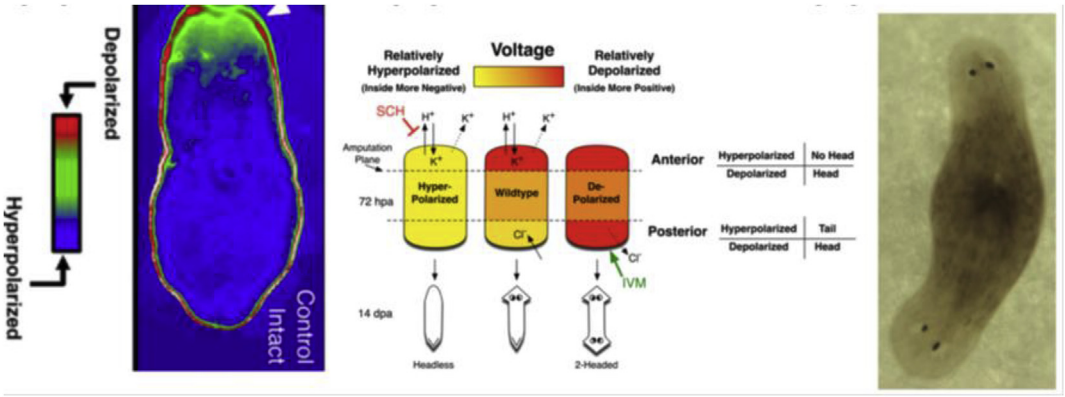

Fig. 1. Bioelectrical signals are instructive both at the single-cell and multicellular levels because they can be transduced into second-messenger responses. Spatio-temporal patterns of electric potential across the anterior-posterior axis of planarian flatworms can be visualized by using voltage reporter dyes (*left*). A bioelectric circuit regulated by proton and potassium channel conductances can establish particular electrical states at each blastema, determining thus the anatomy of the regenerating fragment in the amputated planaria (*center*). This bioelectric circuit can be externally modified by means of genetic and pharmacological techniques. In this way, the biological reprogramming can result in different anatomical outcomes (*right*). Images taken from M. Levin (2014); Molecular bioelectricity: how endogenous voltage potentials control cell behavior and instruct pattern regulation in vivo. *Mol. Biol. Cell* 25 3835–3850 (Levin, 2014).

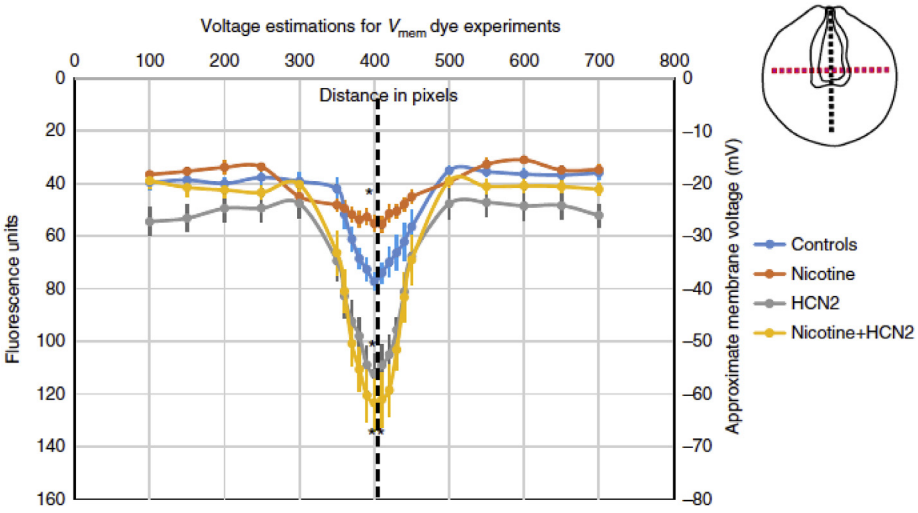

Fig. 2. Voltage reporter dyes reveal the influence of the *HCN2* channel on the rescue of nicotime-induced brain defects by enforcing endogenous voltage pre-patterns. Nicotine participates in the disruption of bioelectrical patterns and exogenous *HCN2* ion channels can restore the endogenous pre-patterns needed for correct brain patterning. The images correspond to stage ~15 *Xenopus* embryos and are obtained along the red dotted line in the inset illustration. The reduction in the fluorescence intensity/membrane voltage pattern along the neural tube (black dotted line in the inset illustration and the graph) is significant in nicotine-exposed embryos in comparison to controls. Clearly, the *Hcn2-WT* mRNA microinjection can enhance these fluorescence intensity/membrane voltage patterns within the neural tube in comparison to controls. Image taken from V. Pai, A. Pietak, V. Willocq, B. Ye, N.-Q. Shi and M. Levin (2018); HCN2 rescues brain defects by enforcing endogenous voltage pre-patterns. *Nat. Commun.* 9998 (Pai et al., 2018).

regionalizations and the resulting biological outcomes can be reprogrammed by appropriate external actions (Cervera et al., 2018a; Levin et al., 2017; Mathews and Levin, 2017).

The membrane is the physical interface between the cell internal functions and the external microenvironment influencing these functions. The ion channels provide the necessary connection between external causes and internal effects or vice versa. The gap junctions and the external microenvironment allow intercellular coupling, offering the possibility that ensemble-averaged magnitudes influence multicellular outcomes. *Could it be possible to establish biophysical controllers for ensembles of coupled non-excitable cells instead of acting at the single-cell level?* If this is the case, cell membrane potentials and ionic currents should be convenient magnitudes for large scale actions, as in computer and brain architectures (Cheney et al., 2014). Following this analogy, the running of a program on a computer is based on the temporal control of voltage and electronic currents at a limited number of physical locations rather than on the detailed local description of billions of transistors and electrical carrier densities.

We use an electrically-focused model to simulate the collective processes that emerge when a group of cells interact bioelectrically on the basis of the transmembrane or *membrane potential* V_{mem} (Cervera et al., 2016, 2018a). This electrical potential difference between the cell inside and the external microenvironment takes negative values, usually from −70 mV (*polarized* cell) to −10 mV (*depolarized* cell). Following an ion channel-based approach, we consider four significant biophysical questions:

i. How could a single-cell bioelectrical state be established?
ii. How could a change in the dynamic cell potential be maintained after a transient perturbation of the cell polarization state?
iii. How could a single-cell contribute to the control of multicellular ensembles based on the spatio-temporal pattern of electrical potentials?
iv. How could oscillatory patterns arise from the single-cell bioelectrical dynamics?

While the above questions have touched upon in our previous studies (Cervera et al., 2018a and 2018b), we now present new results that emphasize the role of electric potential patterns in the control of multicellular ensembles.

Points *i*)-*iv*) are interrelated and tend to arise as *inverse problems* (Lobo et al., 2014; Levin et al., 2017; Cervera et al., 2018a) because we can observe the emerging bioelectrical effects but have only a limited information concerning the single-cell and intercellular coupling causes. In the traditional biochemical approach, this coupling is usually described by the diffusion of signaling ions and molecules. However, the fact is that the transport ions and molecules in solution is influenced by the spatial potential distributions (Levin et al., 2017). In addition, it is likely that extracellular diffusion alone may not allow an efficient propagation of signals without significant distortion (Richardson, 2009) and intercellular bioelectricity is emerging as a fast and robust complementary mechanism. Consistent with this view, we address the above points by emphasizing bioelectrical rather than biochemical signals and using an admittedly simple approach based on two key concepts:

1. The single-cell state is determined by an *inward-rectifying* voltage-gated channel of maximum conductance G_{pol} that promotes the polarized (*pol*) state and an *outward-rectifying* voltage-gated channel of maximum conductance G_{dep} that promotes the depolarized (*dep*) state. While cells express a variety of ion channels with different characteristics, significant overlapping and compensation is necessary for establishing robust electrophysiological properties. Experimentally, voltage-gated channels are central to cell bioelectricity (Kirkton and Bursac, 2011; Yang and Brackenbury, 2013; Djamgoz, 2014; Bates, 2015; Pai et al., 2015; Levin et al., 2017). The fundamental single-cell characteristic considered here is the polarized/depolarized state. Because we introduce only *two generic channels* with opposing effects, similar bioelectrical (*not* biochemical) cell states can be established with different choices of membrane ion channels, which should be an advantage when attempting to externally modify membrane potentials. This question is supported by experimental data

(Blackiston et al., 2009; Levin et al., 2017; Cervera et al., 2018a): altering the balance of key channel conductances is sufficient to establish target V_{mem} distributions that produce the desired biological outcome, strongly suggesting that different experimental causes can lead to a similar bioelectrical effect.

2. The cells in the multicellular ensemble are connected by intercellular *gap junctions* with voltage-gated conductances that act as *bioelectrical transistors* (Chernet et al., 2015; Mathews and Levin, 2017) providing the necessary ensemble plasticity (Fig. 3). The intercellular coupling should be *weak* to allow the spatial regionalization of the electric potential (Cervera et al., 2016; Pietak and Levin, 2017) because the limiting cases of *strong* coupling (isopotential multicellular ensemble) and *zero* coupling (isolated cells) do not allow to store any patterning information. Gap junction regulatory mechanisms make them ideal bioelectrical valves for implementing dynamic and variable connectivity patterns (Palacios-Prado and Bukauskas, 2009).

Experimentally, different membrane potentials are characteristic of basic cell phenomena such as cycle progression, differentiation, and apoptosis (Blackiston et al., 2009; Sundelacruz and Levin, 2009; Krüger and Bohrmann, 2015). The distinct bioelectrical states inherent to cellular ensembles are associated with specific functional outputs (Mathews and Levin, 2017; Krüger and Bohrmann, 2015; Busse et al., 2018). Except for the particular case of neural cells, however, emphasis is usually made on *biochemical* rather than *bioelectrical* cell states (Koseska and Bastiaens, 2017).

Using the approach schematically shown in Fig. 3, we describe how spatio-temporal maps of multicellular electric potentials can be relevant to biological outcomes (Chernet et al., 2015; Pai et al., 2015, 2018; Mathews and Levin, 2017). These multicellular states are modulated by the relative values of the single-cell channel conductances G_{pol} and G_{dep} promoting the polarized and depolarized single-cell states, respectively, and the maximum intercellular conductance G^o of the gap junctions. In this simplified approach, these *effective* conductances simulate the concerted action of many specific channels in the membrane that control the dynamic potential V (Hille, 1992; Kirkton and Bursac, 2011; Chernet et al., 2015; Pai et al., 2015; Mathews and Levin, 2017; Cervera et al., 2018a, 2018b).

This manuscript is organized as follows. First, the single-cell bioelectrical model is presented. Second, the intercellular connectivity between cells that allows multicellular regionalization is discussed. Three biologically-relevant case studies showing the role of electric potential patterns as distributed controllers are then described, with appropriate references to experimental systems. A brief discussion section highlights the main ideas presented and proposes future developments. Finally, two more technical sections describe the model simulations and their limitations.

2. Single-cell bi-stable state

Fig. 4 shows a graphical explanation of how an electric circuit based on only two generic voltage-gated channels inserted in a cell membrane can act as a *bioelectrical memory* characterized by particular values of the potential V_{mem} (Cervera et al., 2016). This phenomenon has been recently identified in a number of systems, such as regenerating planaria in which changes of bioelectric state induce stable changes in regenerative anatomy (Durant et al., 2017). The *Model simulations* section describes the individual characteristics of the channels. In particular, we emphasize that the single-cell bi-stable state is based on the *negative conductance* region of the voltage-gated channel promoting the polarized state. Experimentally, this region can be obtained using e.g. an inward-rectifying potassium channel (Hille, 1992) but other combinations of ion channels and gap junctions can also give bi-stability (Baigent et al., 1997; Cervera et al., 2014; Law and Levin, 2015).

Fig. 4 shows that the single-cell bioelectrical state is regulated by the *relative* values of the channel conductances G_{pol} and G_{dep} which depend both on transcriptional processes and post-translational gating (Cervera et al., 2016). Hence, external perturbations can produce changes in the cell polarization states. These changes can be realized in a controlled way, e.g. by mRNA microinjections, externally-induced blocking of a specific channel conductance, and changes in the microenvironmental ionic

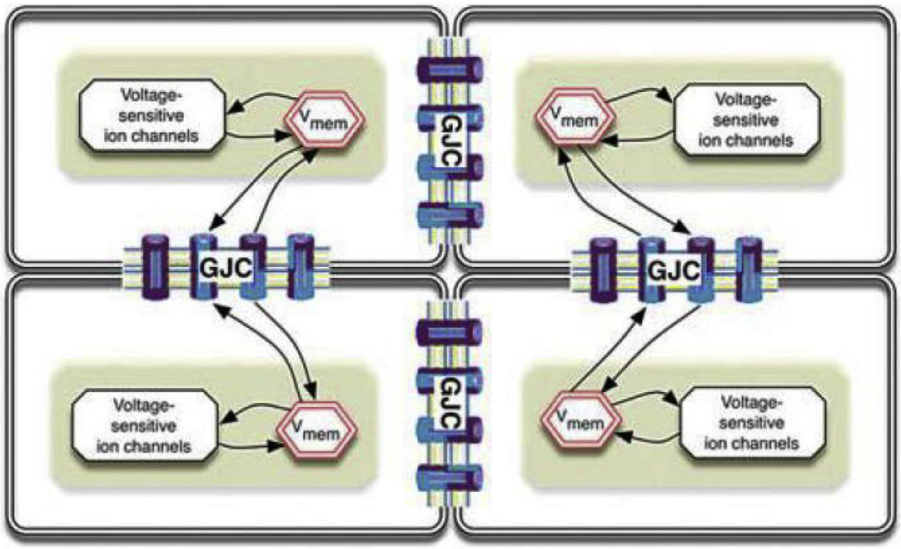

Fig. 3. At the single-cell level, the transmembrane potential V_{mem} influences and is influenced by voltage-sensitive ion channels. In turn, this feedback involves other biological properties such as local pH values and concentrations of ions and signaling molecules. The complex single-cell dynamics is coupled at the multicellular level by intercellular gap junction channels (GJC). As a complementary view to the biochemical approach, we suggest here that this intercellular coupling can help to implement a *distributed control* scheme based on bioelectrical concepts. Image taken from Mustard and Levin (2014). Bioelectrical Mechanisms for Programming Growth and Form: Taming Physiological Networks for Soft Body Robotics *Soft Robot.* 1169–191 (Mustard and Levin, 2014).

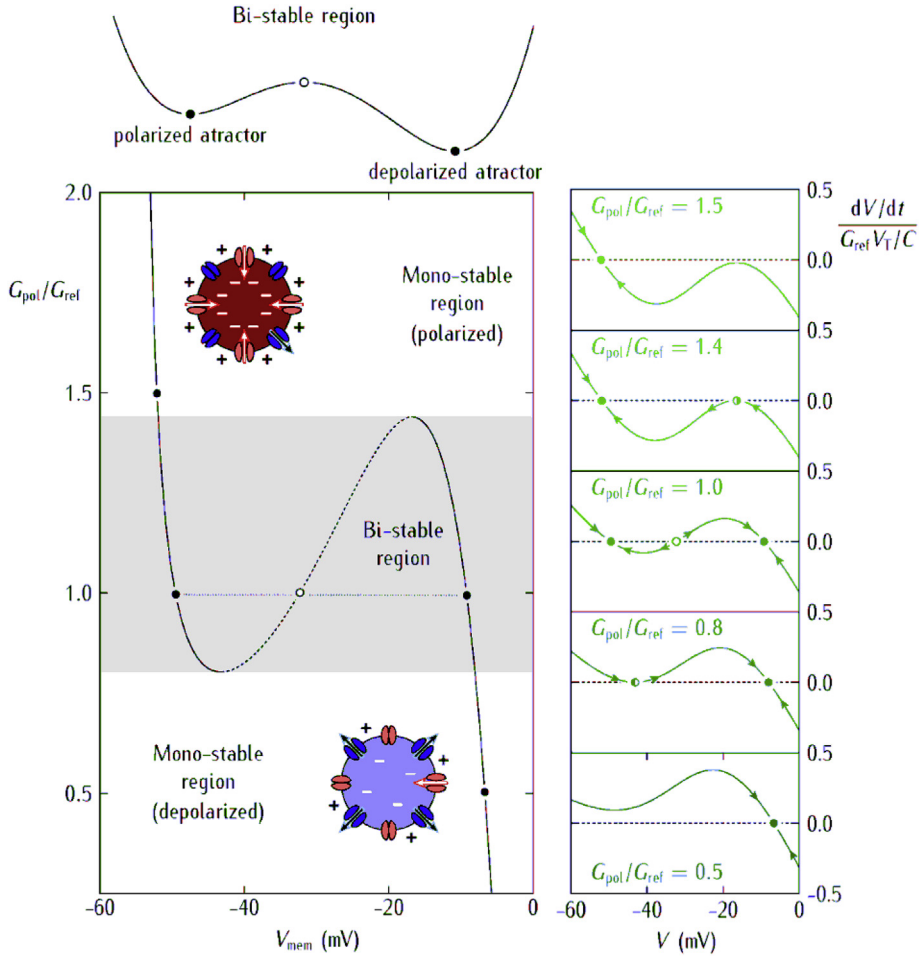

Fig. 4. The single-cell *membrane potential* V_{mem} determines different cell bioelectrical states (*left*) regulated by the channel conductances G_{pol} and G_{dep} of two generic voltage-gated channels that promote the cell polarized (*red*) and depolarized (*blue*) states, respectively. We take $G_{dep} = G_{ref}$ in the figure and change G_{pol}, where G_{ref} is a reference conductance. The change of the *dynamic cell potential* V with time t (*right*) describe the working principle of the memory. For clarity, dV/dt is written in dimensionless form in terms of the cell capacitance C and the constant thermal potential V_T (see the *Model simulation* section). Note the *unstable* value located between the two *stable* polarized and depolarized values of V_{mem} (*full points*). These stable values of V_{mem} depend on the channel conductances and the ionic concentrations inside and outside (external microenvironment) the cell (Hille, 1992; Blackiston et al., 2009; Cervera et al., 2018a).

concentrations. This external modulation of V_{mem} allows establishing the target potential windows necessary to achieve particular biological outcomes (Blackiston et al., 2009; Levin et al., 2017; Pietak and Levin, 2017; Cervera et al., 2018a; Pai et al., 2018). Importantly, in addition to experimental perturbations, these same parameters can be controlled by the cell itself, as well as by multicellular aggregates and tissues in the body, commensal microbiota, parasites, and other physiological inputs.

3. Single-cell bioelectrical state perturbation and recovery

Fig. 5 gives a particular example of how the single-cell of Fig. 4 can be shifted between two stable depolarized and polarized cell states by an *external perturbation* that increases the conductance G_{pol} that promotes the cell polarized state with respect to the conductance $G_{dep} = G_{ref}$ that promotes the depolarized state. The perturbation is maintained for the time interval $5 < t < 10$ s. The changes obtained in the *dynamic* cell potential V (Fig. 5, *up*) attempt to polarize the cell for *weak* (*left*) and *strong enough* (*right*) perturbations. However, the transition between the initial (depolarized) and final (polarized) values of V_{mem} occurs only if the perturbation is strong enough (Fig. 5, *bottom*). In this case, the cell cannot return to its initial depolarized state after termination of the perturbation and then a new polarized state is achieved.

Fig. 5 shows that the two bioelectrical states of Fig. 4 constitute a *memory unit* that can be shifted between the depolarized and polarized values of V_{mem} by external changes of the channel conductances. In particular, the model suggests that a *brief perturbation* occurring over an optimal time window can make a *lasting change* in the cell bioelectrical state. Alternatively, this shift between the two cell polarization states can also be triggered by appropriate changes in the microenvironmental ionic concentrations that regulate V_{mem} (Hille, 1992; Foppen et al., 2002; van Mil et al., 2003; Blackiston et al., 2009). We will show next how the extension of single-cell states to the *multicellular level* can lead to *distributed controllers* that are based on *electrical potential patterns*. To this end, we must describe first the working principles of intercellular gap junctions as voltage-gated ensemble nodes.

4. Intercellular coupling model

The *gap junction* conductance between two neighboring cells is modulated by the difference between their respective cell potentials (Baigent et al., 1997; Chernet et al., 2015; Mathews and Levin, 2017). This characteristic is essential for patterning because adaptive mechanisms acting at the multicellular level must respond to

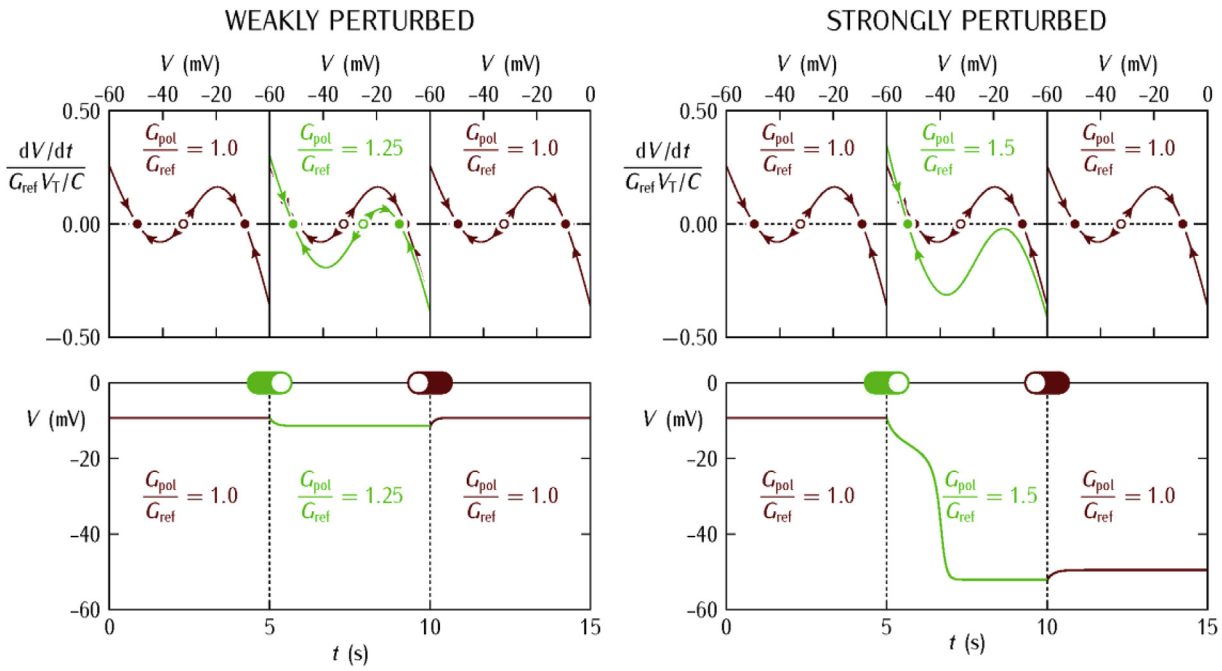

Fig. 5. A weak perturbation caused by an externally-induced change in the relative conductance ratio G_{pol}/G_{dep} is not enough to change the cell polarization state after this stimulus is gone (*left*). On the contrary, the cell polarization can be changed for a strong enough perturbation (*right*). The perturbation concerns a transient increase of the conductance G_{pol} promoting the polarized state with respect to the conductance $G_{dep} = G_{ref}$ promoting the depolarized state. Experimentally, this increase in the relative conductance ratio G_{pol}/G_{dep} can be achieved by microinjection of the specific mRNA (Pai et al., 2018) that encodes the protein corresponding to the channel conductance G_{pol}. Alternatively, the channel conductance G_{dep} can be decreased by using specific blockers (Verdia-Baguena et al., 2012). Note however that these external actions would produce additional *diffusion-reaction* processes characterized by experimental times much higher than those obtained here with a purely electrical approach that assumes abrupt conductance changes at $t = 5$ s and $t = 10$ s.

relative intercellular differences rather than to absolute single-cell magnitudes. Experimentally, the conductance G_{ij} can be approximated by a bell-shaped function (Fig. 6) of the intercellular potential difference $V_i - V_j$ between neighboring cells i and j (Chanson et al., 1993; Tong et al., 2004; Sheldon et al., 2014). In this way, the maximum coupling conductance G^o/G_{ref} is attained for $V_i = V_j$. On the contrary, the intercellular conductance is very small at the frontier between polarized and depolarized regions because the bell-shaped function G_{ij} takes low values when its argument $V_i - V_j$ takes high absolute values (Fig. 6).

Fig. 6 (*right*, c and d) has a solid experimental basis (see e.g. Fig. 3 of Chanson et al., 1993, Fig. 2–6 of Musa et al., 2004, and Fig. 6 of Tong et al., 2004) and is reminiscent of the functional response of the tunnel diode, an electronic device which can work as an amplifier, oscillator, or bi-stable memory element. The low and high conductance states allow for a bi-stable memory while the negative differential conductance region can support multicellular oscillatory phenomena (Cervera et al., 2018b). In this way, the single-cell conductance gating (Fig. 4) together with the intercellular conductance gating (Fig. 6) can regulate the multicellular bioelectrical state on the basis of their plasticity characteristics. In particular, the voltage-gated junction of Fig. 6 switches off electrical communication between cells with different polarization states (Baigent et al., 1997; Baigent, 2003; Cervera et al., 2016), which allows establishing spatial regionalizations based on the differences between the bioelectrical states of neighboring cells (Cervera et al., 2016).

Two experimental facts can provide additional functional roles to gap junctions: (*i*) different connexins with distinct gating behaviors can coexist in intercellular junctions allowing to extend the *dynamic range* of bioelectrical responses (Sheldon et al., 2014) and (*ii*) the gating kinetics of these junctions usually shows different initial and steady state conductance values (Chanson et al., 1993; Tong et al., 2004) which can permit a *frequency-dependent* signal filter. These empirical properties should be especially suitable to establish adaptive responses to the different electrical signals in multicellular ensembles, both biological and artificial.

Following our theoretical program, we discuss now three examples of biological significance. These case studies show that the combination of the single-cell memory of Fig. 4 with the intercellular coupling of Fig. 6 allows for: (*i*) bioelectrical buffering in a small syncytium, (*ii*) spatio-temporal patterns in multicellular aggregates, and (*iii*) synchronized oscillatory phenomena based on *electrical potential patterns* acting as *multicellular controllers*.

5. Bioelectrical buffering

Fig. 7 emphasizes the role of electric potential as a *multicellular controller*. We consider an ensemble (syncytium) formed by a central cell and n neighboring cells. At $t = 0$ s, we assume that the central cell undergoes the externally-induced depolarization of Fig. 7 (*top*). This depolarization is assumed to decrease locally the absolute value of the equilibrium potential E_{pol} corresponding to the ion whose concentration has changed (Cervera et al., 2016). Here, the number n of surrounding cells is a measure of the degree of intercellular coupling between the central cell and its neighbors. The abnormal, depolarized cell can recover the normal polarized state by bioelectrical coupling with the neighboring cells.

In Fig. 7, the uncoupled ($n = 0$) central cell becomes fully depolarized: the cell potential V becomes close to zero (*down*) following the externally-induced depolarization (*top*). On the contrary, cell depolarization is moderate when the central cell has a

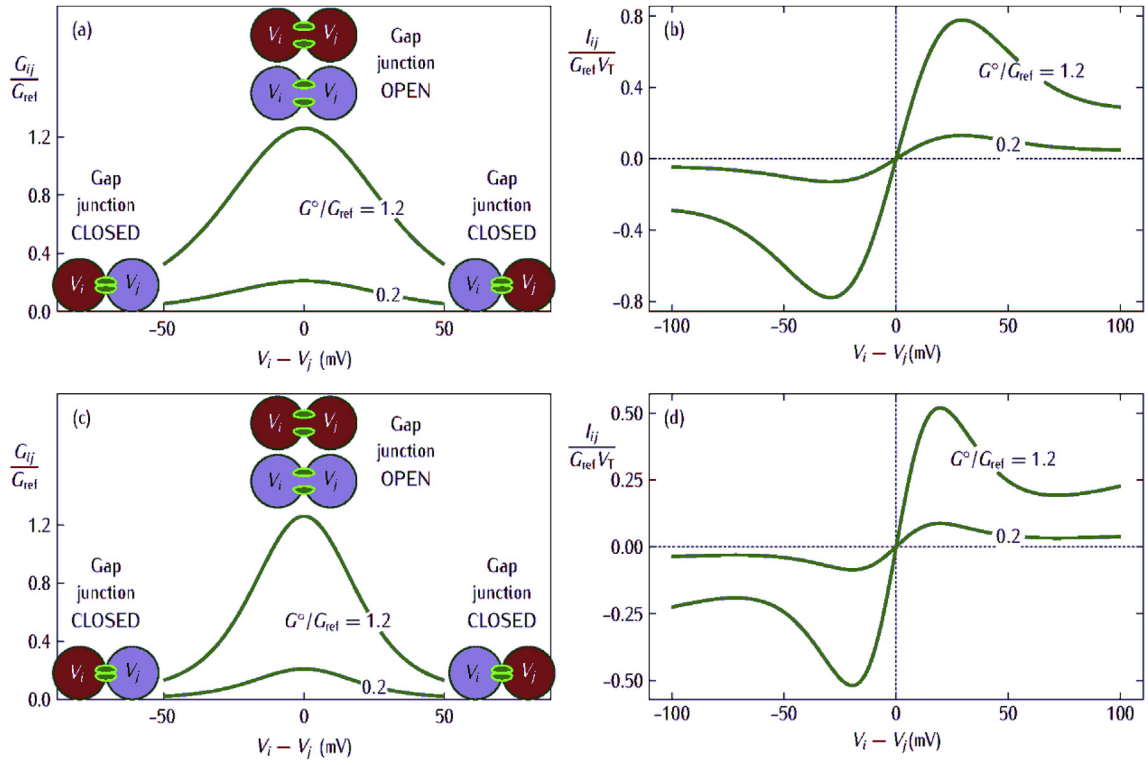

Fig. 6. Experimentally, the gap junction conductance G_{ij}/G_{ref} between two neighboring cells i and j follows a bell-shaped function of the potential difference $V_i - V_j$ (*left*, (a) and (c)) which confers the intercellular plasticity (*right*, (b) and (d)) of the effective nodes in the multicellular ensemble. The curves show two high and low values of the maximum conductance G^o scaled to the reference conductance G_{ref} (Baigent, 2003). This maximum intercellular conductance is attained when the two cells are at the same polarized (*red*) or depolarized (*blue*) potentials. Note that, in addition to this *internal* voltage gating affecting the conductance G_{ij}, the conductance G^o can also be decreased by blocking the junction with *external* agents (Emmons-Bell et al., 2015). The other junction parameters are the potential V_0 that determines the width of the bell-shaped function usually employed to fit the experimental distribution of conductances and the residual conductance. The cases $V_0 = 18$ mV and $G_{res} = 0$ nS (a) and $V_0 = 12$ mV and $G_{res} = 0.05G^o$ (c) are shown. The current-voltage curves of the junction (*right*, (b) and (d)) are obtained as the product $I = G_{ij}(V_i - V_j)$. These curves usually show a non-zero residual conductance (*right*, (d)) in the experimental range studied (Tong et al., 2004).

high number of connected neighbors ($n = 6$). In this case, V is kept close to polarized values (*bottom*) despite the abnormally low potential E_{pol} (*top*). Fig. 7 shows also the dramatically different effects caused by the blocking of the polarizing channel in the cases of the uncoupled and highly-coupled central cell. This blocking begins at $t = 10$ min and is simulated by a slow decrease of the conductance G_{pol} during the time interval $10 < t < 15$ min. The isolated central cell depolarizes completely because of the now dominant conductance $G_{dep} \gg G_{pol}$. On the contrary, the connected central cell recovers the polarized state because of the coupling with the surrounding polarized cells. In this case, the bioelectrical buffering is provided by the average electric potential that acts again as an *ensemble controller* enforcing the isopotentiality of syncytium. In this way, Fig. 7 suggests that the effect of an external perturbation on a multicellular aggregate depends on the internal coupling degree of the cells.

Experimentally, astrocytes are coupled through a network of gap junctions (Ma et al., 2016). One of the roles of this syncytium is to act as a bioelectrical buffer against local changes in the extracellular potassium concentration that might depolarize a particular cell. Thus, the intercellular junctions provide the coupling necessary to achieve network isopotentiality, as suggested by Fig. 7. Although our model is focused only on gap junction currents (Fig. 6) and does not incorporate explicitly the intercellular potassium transference (Huguet et al., 2016; Ma et al., 2016), the results of Fig. 7 reproduce qualitatively the experimental trends reported in Figs. 1I and 3D-G of reference (Ma et al., 2016).

6. Multicellular spatio-temporal patterns

We show next that spatio-temporal patterns of cell electrical potentials can act as *multicellular controllers* encoding specific biological outcomes (Cervera et al., 2018a; Pai et al., 2018). As an illustrative example of experimental interest (Pai et al., 2018), we consider the *two-region* ensemble of Fig. 8 composed of a *ventral depolarized* region characterized by low absolute values of V_{mem} and a *dorsal polarized* region with high absolute values of V_{mem} (Table 1). We establish the bioelectrical communication between these regions via intercellular gap junctions (Fig. 6) and simulate the ensemble evolution for different intercellular coupling degrees (Fig. 8).

Table 1 gives a brief summary of the biophysical parameters used, which are justified in the *Model simulations* section. The parameters for the *dorsal* region correspond to a cell state in the *polarized* mono-stable domain of Fig. 4 because of the relatively high conductance $G_{pol}/G_{ref} = 1.5$ assumed for the time interval $0 < t < 10$ s. On the contrary, the relatively low conductance $G_{pol}/G_{ref} = 1.0$ assumed for the *ventral* region gives *two* stable states of V_{mem} all over the time (Table 1 and Fig. 4).

We consider now a *transient perturbation* which acts only on the *dorsal* region (Fig. 8). To this end, we assume the following time series for the dorsal *pol* channel conductance $G_{pol,\ dorsal}/G_{ref} = 1.0$ ($t = 0$ s), 1.5 ($0 < t < 10$ s), and then back to 1.0 ($t > 10$ s). In this way, the *depolarized* state is established at $t = 0$ s over the whole multicellular ensemble because of the *low* value $G_{pol,\ dorsal}/G_{ref} = 1.0$ *initially* assumed in the dorsal region. At $t > 0$ s, however, the

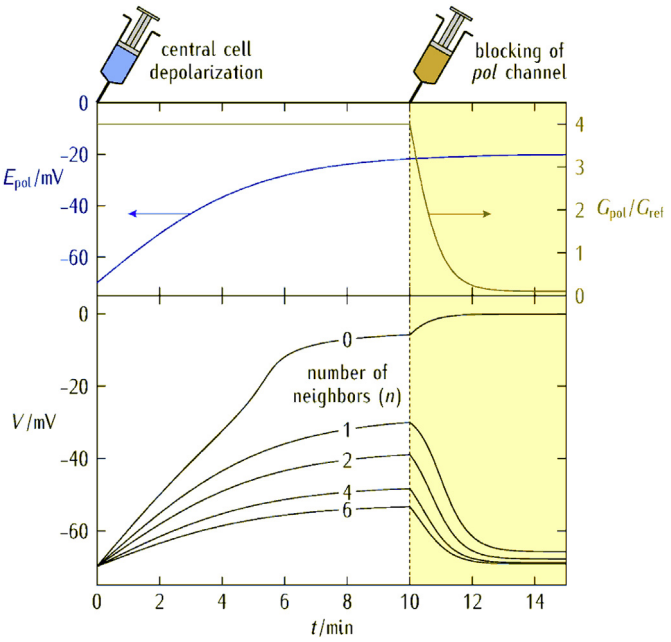

Fig. 7. The depolarization of the central cell due to changes in the concentration of a particular ion in the external microenvironment is simulated by decreasing the absolute value of the equilibrium potential E_{pol} of this ion (Cervera et al., 2016) over the time interval $0 < t < 10$ min (*top*). This externally-induced action provokes the depolarization of the central cell potential V. Because of the controlling role of the electric potential, however, this abnormally low potential V can be normalized for the case of high bioelectrical buffering (high n) that enforces syncytium isopotentiality (*bottom*). Later on, we assume that the polarizing (*pol*) channel is externally blocked by considering a slow decrease of the conductance G_{pol} (*top*) during the time interval $10 < t < 15$ min. Note the different responses obtained for the cases of the uncoupled ($n = 0$) and highly coupled ($n = 6$) central cell. The simulation parameters are $G_{pol}/G_{ref} = 4$, $G_{dep}/G_{ref} = 1$, $E_{pol} = -70$ mV, and $E_{dep} = 0$ mV for the cells and $G^o/G_{ref} = 2$ and $V_0 = 12$ mV for the gap junction.

external perturbation attempts to polarize the dorsal region by increasing $G_{pol,\ dorsal}/G_{ref}$ from 1.0 to 1.5. Note that this perturbed value corresponds to a *polarized* rather than a depolarized dorsal region (Table 1). The perturbation is *finally* retired for $t > 10$ s and thus the cells in the dorsal region recover the initially assumed conductance $G_{pol,\ dorsal}/G_{ref} = 1.0$. This externally-induced process is schematically shown in Fig. 8 (*left* time arrows). As in Fig. 5 for the single-cell case, *would this transient stimulus forcing the dorsal region repolarization be enough to avoid depolarization after the external perturbation is gone?*

Fig. 8 shows that the external perturbation can repolarize the dorsal region only if the intercellular conductance G^o/G_{ref} is *low*. In this *weak* coupling case, the dorsal region remains polarized against the depolarizing action of the ventral region for a long time. On the contrary, for *high* enough intercellular conductances (*strong* coupling case), the dorsal region cannot keep its polarized state after the stimulus simulated by the transient increase of $G_{pol,\ dorsal}/G_{ref}$ is retired. Therefore, the emergence of *different* polarization states in the dorsal and ventral regions is possible only for *weakly-connected* cells. In the opposite case of *high* intercellular conductance G^o/G_{ref}, the dominant ventral region prevents the dorsal region from polarizing giving thus an *isopotential* depolarized ensemble (Fig. 8).

The above bioelectrical model for spatio-temporal signaling can also be applied to long-range rescue by ion channel mis-expression, as shown in Fig. 2 (Pai et al., 2018). This computational approach can explain some of the observed experimental results and predict how experimental perturbations may affect the spatio-temporal dynamics of cell membrane potential patterns. Table 2 and Fig. 9 show a particular example that aims at describing qualitatively the bioelectrical states of the cells in two generic dorsal (*neural*) and ventral (*non-neural*) regions within the multicellular ensemble. As in Fig. 8, the cell states are modulated by the relative values of the single-cell channel conductances G_{pol} and G_{dep} promoting the polarized and depolarized cell states, respectively, together with the relative values of the maximum gap junction conductance G^o and the above single-cell conductances.

Here, we consider the case of an externally-induced polarized patch attempting to polarize the initially depolarized dorsal region (Fig. 9). This patch can represent an *HCN2* ion channel-expressing zone that is externally forced within the depolarized non-neural region, as shown in Fig. 2 (Pai et al., 2018). We attempt describe how the distant communication between the cells in the neural and non-neural regions influence the electric potential pattern that regulates a particular biological outcome - brain patterning here. To this end, we study the effects of the relative size and proximity of the dorsal region representing the neural tube and the externally polarized patch in the ventral region.

Note that we have now split the ventral region into a central and two lateral regions, as indicated in Fig. 9. The three different snapshots of Fig. 9 correspond to the initial zero time (*top*), transient time (*intermediate*), and final steady-state time (*bottom*) cases. In each case, the only difference between the left and right images is the distance of the polarizing patch to the dorsal region. The polarization wave reaches the dorsal region only in the *left* case but not in the *right* one. The blue lines that point to the lateral white dashed lines between the different regions schematically show the resistance exerted by the lateral depolarized regions to the polarizing central wave. In this simulation, the polarizing patch is effective at long distances because the two lateral regions act to prevent the polarizing wave from spreading laterally. In the model, the influence of the gap junctions is based on the potential difference $V_i - V_j$ between two neighboring cells i and j. Hence, the mutual influence between two regions is based on the modification of the cells potentials that serve as a bridge between these regions.

In Fig. 9, the polarizing wave spread depends on:

i) the particular single-cell stable states (*pol* or *dep*; see Table 2) that are possible for the cells in the different regions. In bistable systems, one of the two stable states tends to dominate over the other for the assumed conditions - the conductance ratio G_{pol}/G_{dep} in Table 2;
ii) the shape and size of these regions;
iii) the size and position of the externally polarized patch; and.
iv) the spatial distribution of the intercellular connectivity.

The *bioelectrical anisotropy* is crucial for the spreading of the polarizing wave to the neighboring regions, as observed in the physics of wave propagation through anisotropic media. In this context, artificial tissues could be prepared with bioelectrically heterogeneous regions, with the advantage of incorporating a limited number of ion channels and gap junctions whose functional role is known. This experimental approach can be useful for real biological problems where an understanding of the particular channels entering the biochemical and bioelectric networks, together with some knowledge of the spatial heterogeneities, are desirable for goal-oriented external actions (Churchill et al., 2019).

Note also that, in this purely bioelectrical model, an experimental scenario is possible where the polarization propagates first to a specific region and then this region can spread it to other locations that the initial patch could not convert on its own. This sort of *progressive takeover* depends on the size and properties of the different regions. The observed experimental times, however, can

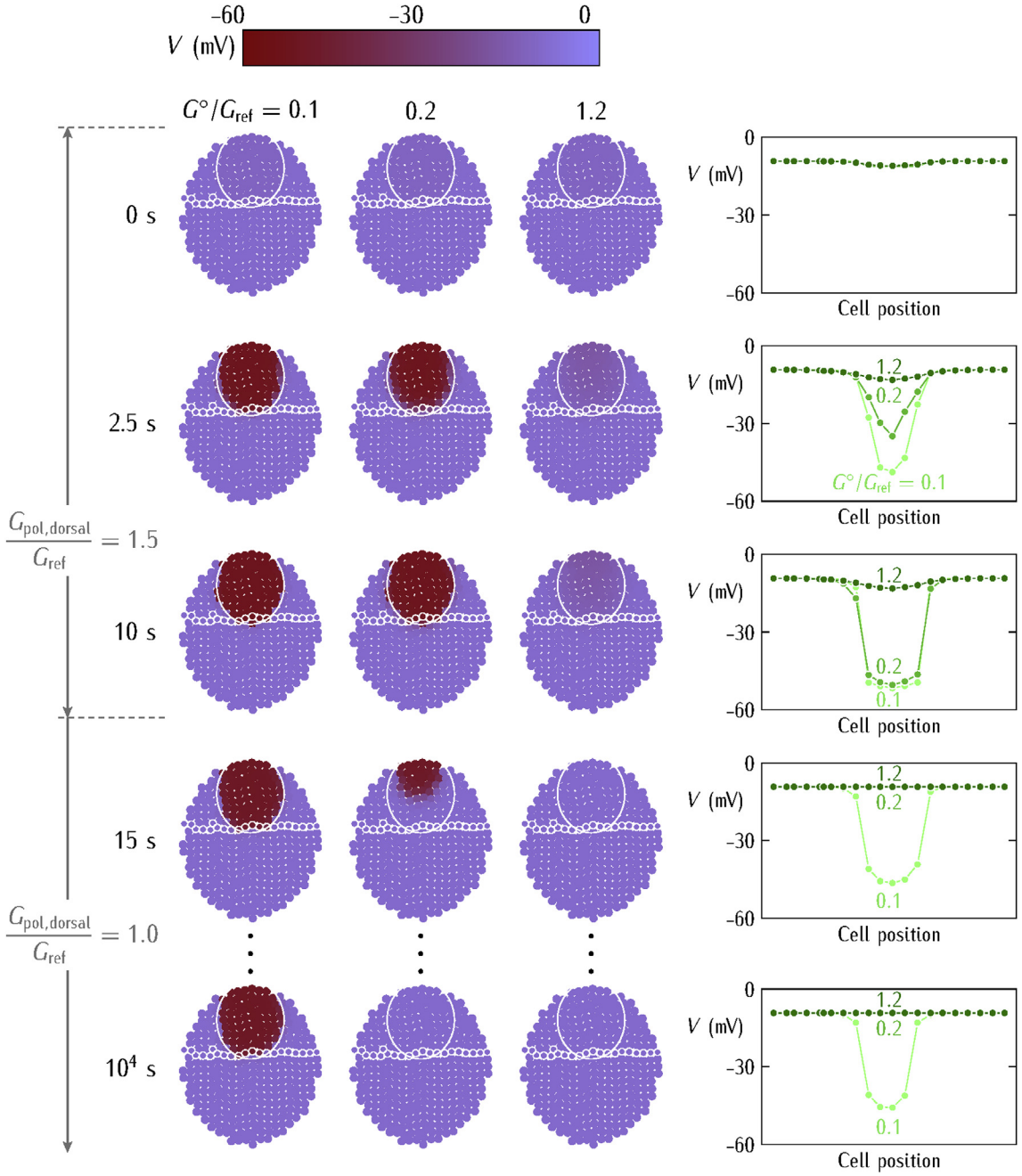

Fig. 8. The spatio-temporal electric potential patterns obtained for the cell parameters of Table 1. Initially ($t = 0$ s), all cells in the ensemble are in the depolarized state characterized by $G_{pol}/G_{ref} = 1.0$ (*left*). At $t > 0$ s, the *pol* channel conductance is increased to $G_{pol,\ dorsal}/G_{ref} = 1.5$ only in the dorsal region. This external perturbation attempts to polarize the initially depolarized dorsal region. At $t > 10$ s, the transient stimulus is retired and the cells in the dorsal region recover the initial conductance $G_{pol,\ dorsal}/G_{ref} = 1.0$. The *snapshots* show the electrical regionalization at different times (*center*) while the *line graphs* show the propagation of the electric potential patterns for the line of cells marked along the ventral–dorsal–ventral regions (*right*).

be significantly longer than those in the simulations where the spreading over a small 10–20 cell diameter-region takes about 10 s only. In particular, longer experimental times should be expected because of the following additional effects:

i) other slow processes (e.g. diffusion + reaction phenomena) may be coupled with fast electrical processes;
ii) real systems might have "stabilizing checkpoints" not accounted for in the model that oppose the spread of the electrical perturbation; and
iii) the number of cells in typical experiments is much greater than that considered here. For instance, a growing monolayer of 10^4–10^5 cells can give responses on the order of hours or days if genetic pathways are incorporated in the model.

With the above limitations, the obtained patterns are of value to qualitatively understand the observed membrane voltage patterns in *Xenopus* embryos (Pai et al., 2018). In particular, the *snapshots* for the dorsal/ventral regionalizations and the *line graphs* for the propagation of the electric potential patterns (Fig. 8) are

Table 1
Summary of the biophysical parameters introduced in the simulations of Fig. 8. The values of the ion channels conductances G_{pol} and G_{dep} and the equilibrium potentials E_{pol} and E_{dep} are given for the two spatial regions considered. The threshold potentials are $V_{th,pol} = V_{th,dep} = -27$ mV and the effective gating charge number is $z = 3$. The distinct single-cell states that are possible for V_{mem} (*pol*, *unstable*, *dep*) in each region are explained in Fig. 4. The gap junction characteristics (Fig. 6) are also given. See also the *Model simulations* section for details.

VENTRAL REGION		DORSAL REGION ($0 < t < 10$ s)	
pol channel	*dep* channel	*pol* channel	*dep* channel
$E_{pol} = -55$ mV	$E_{dep} = -5$ mV	$E_{pol} = -55$ mV	$E_{dep} = -5$ mV
$G_{pol}/G_{ref} = 1.0$	$G_{dep}/G_{ref} = 1.5$	$G_{pol}/G_{ref} = 1.5$	$G_{dep}/G_{ref} = 1.5$
Three cell states are possible in this region with $V_{mem} = -49.5$ mV (*pol*), -32.3 mV (*unstable*), -9.2 mV (*dep*)		Only one cell state is possible in this region with $V_{mem} = -52.1$ mV (*pol*)	

Number of cells: $N = 334$. **Cell capacitance:** $C_i = 100$ pF. **Residual gap junction conductance**: $G_{res}/G_{ref} = 0$. **Potential width of the gap junction conductance:** $V_0 = 18$ mV. **Maximum coupling intercellular conductances:** see the values of G^o/G_{ref} in the columns of Fig. 8. **Initial (*zero time*) membrane potentials:** $V_{mem,i}\,(t = 0) = -9.2$ mV for all cells $i = 1, 2, \ldots, N$.

Table 2
Summary of the biophysical parameters introduced in the simulations of Fig. 9. The values of the ion channels conductances G_{pol} and G_{dep} are given for the four spatial regions considered. The system parameters are those of Table 1 unless stated otherwise. See also the *Model simulations* section for additional details.

Dorsal region		Polarizing patch	
Polarizing channel	Depolarizing channel	Polarizing channel	Depolarizing channel
$E_{pol} = -55$ mV $G_{pol}/G_{ref} = 1.25$ $V_{mem} = -51.2$ mV, -25.0 mV, -11.5 mV	$E_{dep} = -5$ mV $G_{dep}/G_{ref} = 1.5$	$E_{pol} = -55$ mV $G_{pol}/G_{ref} = 2.0$ $V_{mem} = -53.7$ mV	$E_{dep} = -5$ mV $G_{dep}/G_{ref} = 1.0$
Ventral region (*central* region)		**Ventral region (two *lateral* regions)**	
Polarizing channel	Depolarizing channel	Polarizing channel	Depolarizing channel
$E_{pol} = -55$ mV $G_{pol}/G_{ref} = 1.2$ $V_{mem} = -51.0$ mV, -26.4 mV, -10.9 mV	$E_{dep} = -5$ mV $G_{dep}/G_{ref} = 1.5$	$E_{pol} = -55$ mV $G_{pol}/G_{ref} = 0.5$ $V_{mem} = -7.8$ mV	$E_{dep} = -5$ mV $G_{dep}/G_{ref} = 1.0$

Number of cells: $N = 749$. **Cell capacitance:** $C_i = 100$ pF. **Residual gap junction conductance**: $G_{res}/G_{ref} = 0$. **Potential width of the gap junction conductance:** $V_0 = 18$ mV. **Maximum coupling intercellular conductances:** $G^o/G_{ref} = 1$. **Initial (*zero time*) membrane potentials:** $V_{mem,i}\,(t = 0) = -10.9$ mV for all cells $i = 1, 2, \ldots, N$.

qualitatively relevant to recent experiments with embryonic endogenous pre-patterns of electrical potential, as shown in Fig. 2 (Pai et al., 2015, 2018). In addition, the simulations show that the particular spatial distribution of the intercellular connectivity will influence the effectivity of externally-induced changes (Fig. 9). This connectivity can be modified by transcriptional and translational external actions (Aasen et al., 2016) together with the post-translational blocking of the intercellular conductance G^o/G_{ref} using specific molecules (Emmons-Bell et al., 2015).

In conclusion, Figs. 8 and 9 show that the bioelectrical states of the cells in the dorsal region can be influenced at the *ensemble level* by the neighboring cells in the ventral region because of the long-distance transduction of electrical signals through the intercellular junctions. This fact suggests that different bioelectrical patterns corresponding to distinct biological outcomes could be implemented by externally-induced *dynamic changes* in the junction states (Cervera et al., 2018b). Experimentally, spatio-temporal electric potential patterns have been dynamically established by modulating the intercellular coupling with the result of different anatomical patterning outcomes in planaria (Emmons-Bell et al., 2015; Durant et al., 2018). Once again, these results emphasize the role of electric potentials as *distributed controllers* of multicellular ensembles (Cervera et al., 2016, 2018b; Pietak and Levin, 2017).

7. Multicellular oscillatory and synchronization phenomena

We consider now the case of large-scale bioelectrical synchrony regulated by a dynamic intercellular connectivity (Cervera et al., 2018b), extending the spatial control discussed above to temporally-extended patterns. As in the case of neural networks, we suggest that oscillatory electric potential patterns can contribute to the control of non-excitable cell ensembles. To this end, we make use of the interplay between the biochemical and bioelectrical signals (Cervera et al., 2016) and assume the single-cell parameters to be in the oscillatory regime described with detail previously (Cervera et al., 2018b).

Fig. 10 considers first the case of the single-cell. Concerted oscillations of the *pol* and *dep* channel protein concentrations make the corresponding conductances to oscillate (Cervera et al., 2018b). Therefore, the resulting cell potential also oscillates because of the feedback between biochemical and bioelectrical signals. Phase diagrams showing the particular system parameters that allow the *coupled bioelectrical and biochemical oscillations* have also been previously described (Cervera et al., 2018b).

Fig. 11 extends the results of Fig. 10 to multicellular ensembles (Cervera et al., 2019). Uncoupled (*left*, *bottom*) and locally coupled (*right*, *bottom*) multicellular ensembles are shown. In the latter case, the central cells are highly coupled while the cells in the two surrounding regions are uncoupled.The spatial maps of frequencies correspond to the oscillatory cell potentials obtained for a spatially-random bimodal distribution of single-cell frequencies (*top*). Note the long-range synchronization achieved by the central cells, as opposed to the independent oscillations characteristic of the uncoupled cells in the rest of the ensemble (*right*, *bottom*). This result clearly suggests that different patterns of cell connectivity would give distinct patterns of oscillatory cell potentials. In this sense, multicellular information can be encoded not only with regard to space but also with regard to timing (Cervera et al., 2019).

The synchronization of single-cell genetic and electrical oscillators (Fig. 10) allows the multicellular ensemble to establish coherent temporal rhythms. These collective phenomena can lead

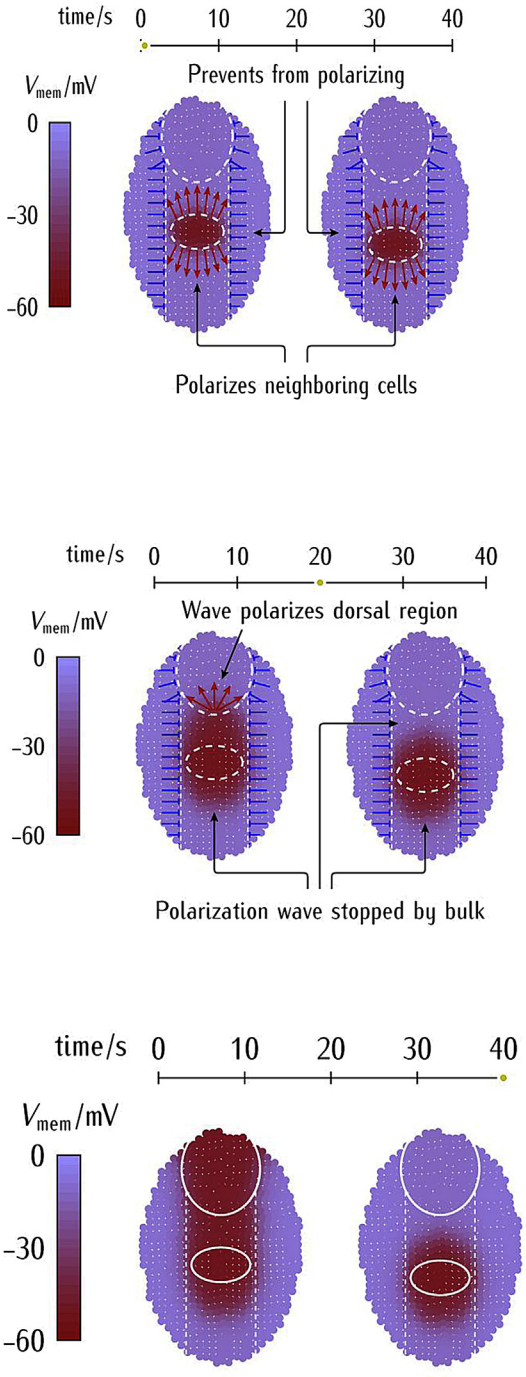

Fig. 9. The spatio-temporal electric potential patterns obtained for the cell parameters of table 2. Note the difference with respect to the simulations of Fig. 8: we have now split the ventral region into a central and two lateral regions. The three snapshots correspond to the initial zero time (*top*), transient time (*intermediate*), and final steady-state time (*bottom*) cases. In each case, the difference between the left and right images is the distance of the polarizing patch to the dorsal region. The blue lines that point to the lateral white dashed lines between the different regions schematically show the resistance exerted by the lateral depolarized regions to the polarizing central wave.

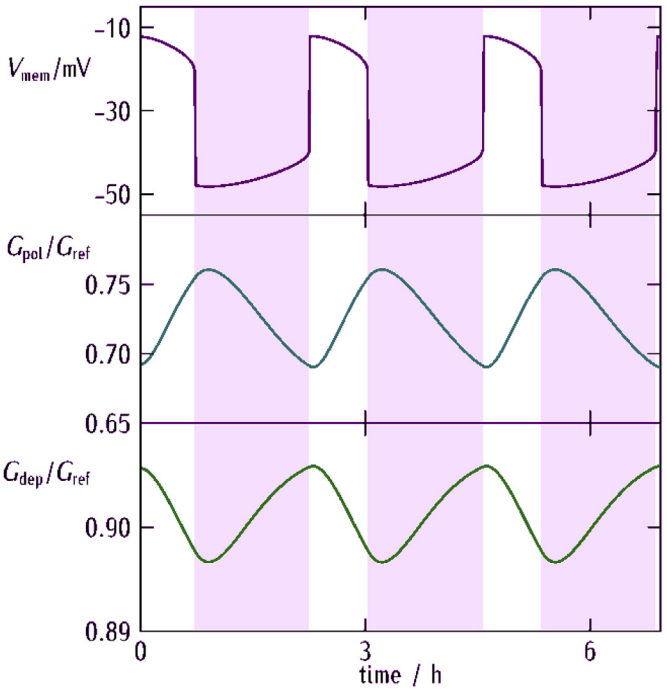

Fig. 10. Single-cell bioelectrical oscillations for the electric potential (*top*) and the channel protein conductances (*intermediate* and *bottom*) can occur for a range of the cell parameters that characterize the coupled bioelectrical and biochemical oscillations (Cervera et al., 2018b).

to patterning based on oscillations (Morelli, 2012). In particular, spatially-structured oscillatory cell populations (Mehta and Gregor, 2010; Shimojo and Kageyama, 2016; Tsiairis and Aulehla, 2016) can be obtained by introducing pre-patterns of genetic rate constants and junction conductances; see references (Cervera et al., 2018a, 2018b) for details. Fig. 11 emphasizes the latter case: coupled cells within a particular region of the multicellular ensemble share the same oscillatory state which is different from those cells in the uncoupled neighboring regions (*bottom*, *right*). It should be noted that these coherent oscillations can emerge in the heterogeneous ensemble of non-neural cells without any centralized coordination, provided that the single-cell parameters are in the oscillatory regime (Cervera et al., 2018b). Interestingly, the cells can coordinate their individual states using both spatial coordinates and time frequencies.

The crucial role of voltage-gated gap junctions in oscillatory and synchronization phenomena has been noted experimentally in the uterus muscle cells showing a coordinated contraction during delivery (Sheldon et al., 2014). Here, different voltage-gated connexin proteins act as electrical connections between neighboring cells. The degree of intercellular coupling modulates the synchronization during contraction, in qualitative agreement with the results of Fig. 11. However, the experimental case is more complex because of the concerted action of two different connexion proteins (Sheldon et al., 2014).

In addition, the single-cell cycle is characterized by oscillatory polarized and depolarized V_{mem} values (Blackiston et al., 2009). Experimentally, the inhibition of specific channels has been related to cell cycle arrest and cease of oscillatory V_{mem} behavior. Also, changes in voltage-gated channels expression and/or function have been considered a cause and/or consequence of changes in V_{mem}. In this context, Fig. 10 provides a physical mechanism for the interplay between the channel protein conductances and oscillatory membrane potentials. In addition, Fig. 11 suggests that a spontaneous or externally induced inhibition of the local intercellular coupling over a small multicellular region should decouple this region from the rest of the ensemble, breaking thus the bioelectric synchronization among cells. This situation can be relevant to both cancer (Chernet

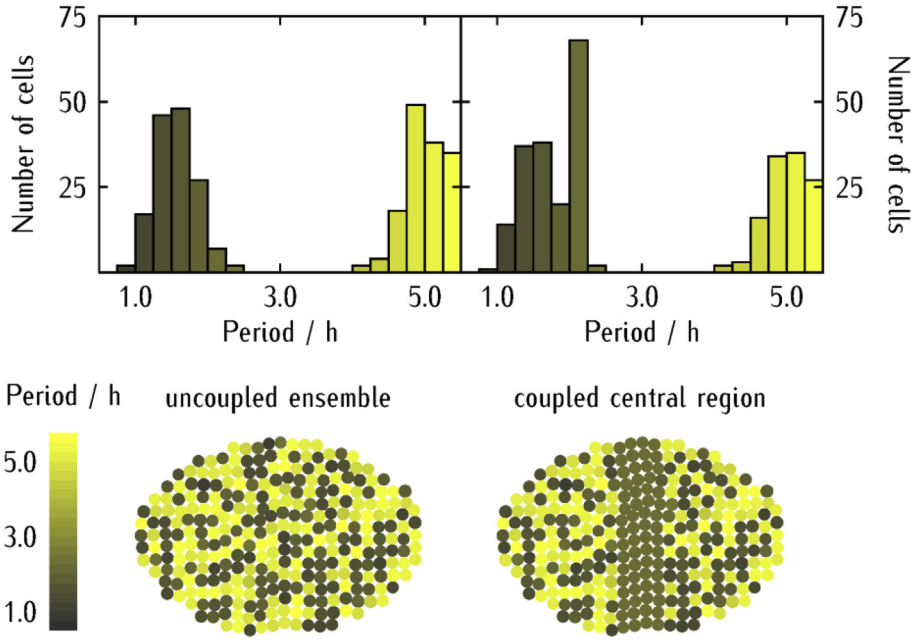

Fig. 11. The frequency maps show that the synchronization of membrane potentials is not possible for uncoupled cells with junction conductance $G^o/G_{ref} = 0$ (*bottom*, *left*). On the contrary, regional synchronization can occur in the case of a coupled central region with $G^o/G_{ref} = 0.5$ surrounded by two uncoupled regions where $G^o/G_{ref} = 0$ (*bottom*, *right*). In both cases, spatially random bimodal distributions of single-cell frequencies are assumed (*top*, *left* and *right*). These frequencies depend on the particular genetic rate constants of each individual cell (Cervera et al., 2018b). In the maps, the periods of oscillating cells are given by their colors.

and Levin, 2013) and changes in species-specific regenerative patterning (Emmons-Bell et al., 2015).

Remarkably, it is the *average potential* established within the coupled multicellular region that allows the coherent oscillations of Fig. 11. In principle, it is conceivable that different regions of interconnected cells may establish *multicellular memories* via slow oscillatory patterns (Cervera et al., 2018b). Note again that the voltage-gated junctions act here as *node bioelectrical transistors* (Fig. 6) providing the junction plasticity needed for a *spatially distributed control*. The regulation of this large-scale synchrony by the dynamic intercellular connectivity produces *slow-wave* potentials (Cervera et al., 2018b) loosely reminiscent of the transient oscillatory states in the brain (Battaglia and McNaughton, 2011). Additional experimental studies relevant to this question are reported in references (Kirkton and Bursac, 2011; McNamara et al., 2016).

8. Multicellular ensemble characteristic times

The fact that the experimental regionalizations take on the order of hours clearly suggests that bioelectricity should be coupled with much slower diffusional and transcriptional processes. We consider next the different characteristic times of the multicellular ensemble. The ratio C_i/G_{ref} gives a typical single-cell electrical time in the second timescale for capacitances and conductances in the ranges $C_i = 10–100$ pF and $G_{ref} = 0.1–1$ nS (Cervera et al., 2016), respectively. Note that this electrical time can be increased significantly for the multicellular spatio-temporal patterns to develop (Fig. 8). In contrast, the cell genetic processes incorporated in Figs. 10 and 11 are much slower because typical transcription, translation, and degradation rate constants give times on the order of hours (Cervera et al., 2016; Cervera et al., 2018a).

Typical diffusional times should take intermediate values between the above electric and genetic characteristic times. For instance, the diffusion time L^2/D can be in the range 10 min – 1 h for a length $L = 10^{-3}$ m (about 100 cells) and diffusion coefficients in the range $D = 10^{-10} - 10^{-9}$ m^2/s. In the simulations, we have implicitly assumed that relatively fast bioelectrical relaxations in the minute timescale can assist the relatively slow spatial redistributions of signaling ions (e.g., Ca^{2+}) and charged molecules (e.g., serotonin and butyrate) taking place in the hour time scale. In the long term, it is the coupling of the local signaling molecules concentrations with very slow genetic processes occurring in higher time scales that will produce the final biological outcomes (Cervera et al., 2018b). Thus, the spatio-temporal potential distributions of Figs. 8, 9 and 11 can be seen as *electric footprints* for the signaling ions and molecules distributions that will eventually influence crucial biochemical pathways (Cervera et al., 2018a). It is in this way that *spatially-distributed control* via *bioelectricity* could help establish, maintain, and improve the robustness of diffusional gradients.

We note also that the coupling among bioelectricity, diffusional processes, and genetic networks may provide some additional benefits concerning the unavoidable local fluctuations of signaling ions and molecules if cells use electrically-established directional values of average concentrations (Zhang and Levin, 2009) over a long time to regulate genetic processes (Cervera et al., 2018b). In addition, because the establishment of local concentrations should be much faster than the above cell averaging times, steady-state signal concentrations can be used in simulations focused on comparatively slow genetic responses (Olimpio et al., 2018). This simplified picture could however be compromised if the genetic responses involve the transcription of ion channel proteins regulating in turn cell bioelectricity.

9. Discussion

As a *complementary* approach to the currently dominant biochemical description, we have shown that the ion channels and gap junction proteins of non-excitable cells can allow instructive

multicellular bioelectrical patterns. Experimentally, the spatio-temporal distributions of many signaling ions and molecules that regulate crucial biochemical pathways are influenced by multicellular maps of electric potentials. In this sense, these maps can indirectly act as *distributed controllers* that allow encoding particular spatial patterns (Cervera et al., 2016, 2018a; Pietak and Levin, 2017) to be decoded by the multicellular system as biological outcomes, as shown by Levin and coworkers (Chernet et al., 2015; Emmons-Bell et al., 2015; Pietak and Levin, 2017; Busse et al., 2018; Pai et al., 2018). There are important parallels between these types of memory and controller dynamics that occur during cognitive processing in brains, and more ancient programs that enable pattern regulation in somatic tissues (Pezzulo and Levin, 2015).

The model incorporates two central bioelectrical concepts: the single-cell voltage-regulated conductances G_{pol} and G_{dep} promoting the polarized and depolarized states and the intercellular coupling conductance G^{o}. Scaling these conductances to the reference value G_{ref} permits a qualitative description of electrical patterns. These patterns are determined not only by the single-cell characteristics (Figs. 4 and 5) but also by the *context-dependent* bioelectrical dynamics of intercellular junctions (Figs. 3, 6 and 7). In this way, the biophysical outcomes are not encoded simply in steady images but in the time-dependent (Figs. 8 and 9) and oscillatory (Fig. 11) bioelectrical patterns that frame the multicellular states (Cervera et al., 2018b).

However, the simulations suggest also that external actions addressed to establish target outcomes can be effective only within a *limited range* of experimental conditions. The intensity and time window of the perturbation (Figs. 4 and 5) and the degree of intercellular coupling (Figs. 3, 6 and 7) are especially important. In addition, bioelectrical and biochemical signals should act in concert for the transitions to be effective in real cases. While we have emphasized here the case of *voltage-gated* ion channels and junctions because they allow fast and long range signal transmission compared with purely diffusional processes, the above ideas can also be implemented with chemical and optical gating (Kirkton and Bursac, 2011; Emmons-Bell et al., 2015; Chernet et al., 2016; McNamara et al., 2016; Pai et al., 2018).

Endogenous bioelectric gradients have emerged as instructive agents for morphogenetic processes that are ruled by the dynamic intercellular connectivity. In real cases, the present approach must be complemented with many structural details that escape a mean-field regulation. However, the simulations may guide experimental procedures attempting to establish and maintain bioelectrical patterns over small regions, such as those that have been used to normalize tumors and induce repair of brain defects (Chernet et al., 2015; Mathews and Levin, 2017; Pai et al., 2018).

10. Limitations of the model

Our bioelectrical description is a *complementary approach* to traditional biochemical models, with the following limitations. Figs. 5, 8 and 9 consider fast, purely electric changes of the channel and junction conductances following the application of an external perturbation which takes seconds, an assumption that may not be valid in most experimental cases. On the contrary, Figs. 7 and 10 involve much longer time responses because of the slow diffusional responses of the ionic concentrations and equilibrium potentials (Fig. 7) which take minutes here, and the interplay between bioelectrical and biochemical signals (Fig. 10), which takes hours here. Certainly, external stimuli such as the microinjection of a specific mRNA and the introduction of blocking agents acting on particular channels will take *longer experimental times* than the purely bioelectrical responses of Figs. 5, 8 and 9 because of the slow *diffusion-reaction* processes associated with the local redistribution of signaling ions and molecules. We have indirectly introduced some of the above effects previously by assuming *ad hoc* local distributions of effective transcription rates (Cervera et al., 2016, 2018b). Despite these limitations, a general conclusion should still be valid: since the spatio-temporal maps of electrical potentials influence the distribution of signaling ions and molecules such as calcium and serotonin, the *spatial regionalizations* of Figs. 8, 9 and 11 should contribute to the development of *different biological outcomes* (Chernet et al., 2015; Pai et al., 2015, 2018; Mathews and Levin, 2017).

In addition, we have assumed implicitly in Figs. 8 and 9 that the external microenvironment acts as a sort of *bioelectrical buffer* that fixes the ionic concentrations and that the inner cell concentrations are kept constant, e.g. by the action of ion pumps (Hille, 1992). A *spatially inhomogeneous* external microenvironment contributing to multicellular patterning (Meinhardt, 2012) could be introduced indirectly in the model by assuming that the equilibrium potentials E_{pol} and E_{dep} of Table 1 change locally with the external ionic concentrations (see the *Model simulations* section). In addition, extensions of the two generic ion channels used here to other channels and pumps are possible (O'Leary et al., 2014; Law and Levin, 2015; Pietak and Levin, 2017). Alternatively, other models incorporating additional bioelectrical effects have recently been developed (Cervera et al., 2016, 2018a; McNamara et al., 2016; Pietak and Levin 2016, 2017; Brodsky and Levin, 2018; Pai et al., 2018).

In real cases, the activation of particular genetic and epigenetic pathways should often involves *biochemical* signaling molecules such as neurotransmitters acting in concert with the purely *bioelectrical* signals emphasized here (Mathews and Levin, 2017). Hence, *extensions of this theoretical approach to include relevant biochemical molecules and pathways are necessary to quantitatively describe real experimental problems* (Cervera et al., 2016, 2018a; Pietak and Levin, 2017; Pai et al., 2018). These model extensions can eventually lead to multiple *bi-stable* and *switching* phenomena. For instance, the specific channels and transporters that regulate the distribution of the signaling molecules between the inside cell and the external microenvironment can be voltage-gated and thus their functions would depend on the cell polarization state (Paré et al., 2017). In addition, local time-dependent fields can permit an electrically-modulated redistribution of signaling molecules such as serotonin and butyrate because these molecules are charged and can also be involved in facilitated transport mechanisms (Mathews and Levin, 2017).

Note that our *ion channel-centered approach* to bioelectrical patterning in non-excitable cells is based on the single-cell multistability of Fig. 4 (Cervera et al., 2014, 2016). In particular, it is the cell bi-stability together with that of the GJs in Fig. 6 that allows for the sharp electric potential regionalizations obtained. In real cases, the slow diffusion of signaling molecules and ions, together with additional cell control processes, should lead to much longer times and more diffuse electrical regionalizations (Mathews and Levin, 2017). Also, the model ignores other nerve-dependent and blood-mediated signaling effects that may also be important. In addition, biomechanical processes and biochemical mechanisms producing inhomogeneous distributions of signaling molecules are commonplace in biological patterning (Richardson, 2009; Meinhardt, 2012; Morelli et al., 2012). These mechanisms can be based e.g. on different signaling molecules experiencing reaction-diffusion phenomena together with local self-enhancement and long-range inhibition (Meinhardt, 2012).

With the above limitations, we have tried to emphasize that single-cell bioelectrical states are not exclusively determined by the transcriptional and translational processes regulating the ion channel protein levels together with the post-translational channel

gating; rather, these individual states should be significantly influenced by the collective phenomena resulting from the intercellular coupling (Fig. 7–9 and 11). In this conceptual scheme, external perturbations on specific single-cell channels and junctions can trigger shifts between multicellular states corresponding to *system attractors* in a biological *phase space* (Koseska and Bastiaens, 2017; Mathews and Levin, 2017). Learning to manipulate these system-level properties can be an important component of future efforts to normalize disease states in a range of applications, ranging from traumatic injury to cancer, using ion channel drugs in blends designed to act as so-called electroceuticals (Tuszynski et al., 2017; Churchill et al., 2019). Similarly, development and analysis of quantitative models that assist in the design of bioelectric circuits will greatly augment efforts to design living cellular machines and engineered bioelectric tissues with desired patterning and functionality (Kamm and Bashir, 2014; McNamara et al., 2016, 2018).

Funding

J C and S M thank the financial support of the Ministerio de Ciencia, Innovación y Universidades and the European Regional Development Funds (FEDER), project No. PGC2018-097359-B-100. M L and V P gratefully acknowledge support by an Allen Discovery Center award from The Paul G. Allen Frontiers Group (No. 12171), the G. Harold and Leila Y. Mathers Charitable Foundation (No. TFU141), the Templeton World Charity Foundation (TWCF0089/AB55), and the National Science Foundation IGERT (DGE-1144591).

Appendix. Model simulations

We use a basic version of a biophysical model previously proposed (Cervera et al., 2016, 2018a) in Fig. 6–9. This model ignores the genetic and bioelectrical feedback at the single-cell level and focuses only on the electrical characteristics. This is not the case of Figs. 10 and 11 where the genetic description is explicitly included (Cervera et al., 2016, 2018a). The dynamic cell potential V is regulated by the channel conductances G_{pol} and G_{dep} and the equilibrium potentials E_{pol} and E_{dep}. These potentials do not change with time provided that the intracellular and extracellular ionic concentrations are approximately constant. Note that this assumption is not considered in Fig. 7. The dynamic cell potential V can show two values V_{mem} that correspond to the polarized and depolarized bioelectrical states (Figs. 4 and 5; Table 1).

The rationale behind the model is that the *single-cell state* can be modulated at the *ensemble level* because of the coupling with the neighboring cells. This coupling is provided by the junction conductance G_{ij} that permits the intercellular electric currents (Cervera et al., 2016) and the transference of signaling molecules (Cervera et al., 2017) between adjacent cells (Figs. 3 and 6). In particular, every central cell i experiences the *electric potential* due to its nearest-neighbor cells. Experimentally, G_{ij} is a bell-shaped function of the potential difference between cells i and j characterized by a maximum conductance G^{o}, a residual conductance G_{res}, and a potential V_0 that gives the width of the experimental distribution of conductances (Fig. 6). The single-cell and intercellular coupling conductances are expressed in terms of a common reference value G_{ref} to allow comparison. Large values of $G^{\mathrm{o}}/G_{\mathrm{ref}}$ give isopotential regions while low values of $G^{\mathrm{o}}/G_{\mathrm{ref}}$ give isolated cells with no bioelectrical communication.

The potential V_i of cell i evolves with time t due to the single-cell channel currents $I_{\mathrm{pol},i}$ and $I_{\mathrm{dep},i}$ together with the intercellular current, regulated by G_{ij} and $V_i - V_j$, which is calculated for the nearest neighbors cells j around the central cell i. The equations for the currents $I_{\mathrm{pol},i}$ and $I_{\mathrm{dep},i}$ qualitatively describe the observed experimental trends in terms of a small number of phenomenological parameters (Cervera et al., 2016). In Table 1, we assume the effective gating charge number $z = 3$ and the threshold potential $V_{\mathrm{th,pol}} = -V_{\mathrm{T}}$ for the voltage-gated channels. Here, $V_{\mathrm{T}} = RT/F = 27$ mV is the thermal potential, where R is the gas constant, T is the temperature, and F is the Faraday constant (Hille, 1992). The N cells in the ensemble form an elliptic monolayer initially at the same potential $V_i(t = 0)$, with $i = 1,\ldots, N$ (Figs. 8 and 9). The evolution of the system for time $t > 0$ is given by the N equations for the cell potentials (Cervera et al., 2016).

References

Aasen, T., Mesnil, M., Naus, C.C., Lampe, P.D., Laird, D.W., 2016. Gap junctions and cancer: communicating for 50 years. Nat. Rev. Canc. 16, 775–788.
Baigent, S., Stark, J., Warner, A., 1997. Modelling the effect of gap junction nonlinearities in systems of coupled cells. J. Theor. Biol. 186, 223–239.
Baigent, S., 2003. Cells coupled by voltage-dependent gap junctions: the asymptotic dynamical limit. Biosystems 68, 213–222.
Baluška, F., Levin, M., 2016. On having No head: cognition throughout biological systems. Front. Psychol. 7, 902.
Bates, E., 2015. Ion channels in development and cancer. Annu. Rev. Cell Dev. Biol. 31, 231–247.
Battaglia, F.P., McNaughton, B.L., 2011. Polyrhythms of the brain. Neuron 72, 6–8.
Blackiston, D.J., McLaughlin, K.A., Levin, M., 2009. Bioelectric controls of cell proliferation: ion channels, membrane voltage and the cell cycle. Cell Cycle 8, 83527–83536.
Brodsky, M.Z., Levin, M., 2018. From Physics to Pattern: Uncovering Pattern Formation in Tissue Electrophysiology ALIFE 2018: the 2018 Conference on Artificial Life Tokyo 351–358.
Busse, S.M., McMillen, P.T., Levin, M., 2018. Cross-limb Communication during Xenopus Hind-Limb Regenerative Response: Non-local Bioelectric Injury Signals Development, vol. 145, p. 164210.
Cervera, J., Alcaraz, A., Mafe, S., 2014. Membrane potential bi-stability in non-excitable cells as described by inward and outward voltage-gated ion channels. J. Phys. Chem. B 11, 12444–12450.
Cervera, J., Meseguer, S., Mafe, S., 2016. The interplay between genetic and bioelectrical signaling permits a spatial regionalisation of membrane potentials in model multicellular ensembles. Sci. Rep. 6, 35201.
Cervera, J., Meseguer, S., Mafe, S., 2017. MicroRNA intercellular transfer and bioelectrical regulation of model multicellular ensembles by the gap junction connectivity. J. Phys. Chem. B 121, 7602–7613.
Cervera, J., Pietak, A., Levin, M., Mafe, S., 2018a. Bioelectrical coupling in multicellular domains regulated by gap junctions: a conceptual approach. Bioelectrochemistry 123, 45–61.
Cervera, J., Meseguer, S., Mafe, S., 2018b. Intercellular connectivity and multicellular bioelectric oscillations in non-excitable cells: a biophysical model. ACS Omega 3, 13567–13575.
Cervera, J., Manzanares, J.A., Mafe, S., Levin, M., 2019. Synchronization of bioelectric oscillations in networks of non-excitable cells: from single-cell to multicellular states. J. Phys. Chem. B 123, 3924–3934.
Chanson, M., Chandross, K.J., Rook, M.B., Kessler, J.A., Spray, D.C., 1993. Gating characteristics of a steep voltage-dependent gap junction channel in rat schwann cells. J. Gen. Physiol. 102, 925–946.
Cheney, N., Clune, J., Lipson, H., 2014.). In: Evolved Electrophysiological Soft Robots Proceedings of the Fourteenth International Conference on the Synthesis and Simulation of Living Systems Artificial Life Conference (ALIFE 2014. doi.org/10.7551/978-0-262-32621-6-ch037.
Cheney, N., Bongard, J., Lipson, H., 2015. Evolving Soft Robots in Tight Spaces Proceedings of the 2015 Annual Conference on Genetic and Evolutionary Computation, vol. 15. GECCO, pp. 935–942.
Chernet, B.T., Levin, M., 2013. Transmembrane voltage potential is an essential cellular parameter for the detection and control of tumor development in a Xenopus model. Dis. Model Mech. 6, 595–607.
Chernet, B.T., Levin, M., 2014. Transmembrane voltage potential of somatic cells controls oncogene-mediated tumorigenesis at long-range. Oncotarget 5, 3287–3306.
Chernet, B.T., Fields, C., Levin, M., 2015. Long-range gap junctional signaling controls oncogene-mediated tumorigenesis in Xenopus laevis embryos. Front. Physiol. 5, 519.
Chernet, B.T., Adams, D.S., Lobikin, M., Levin, M., 2016. Use of genetically encoded, light-gated ion translocators to control tumorigenesis. Oncotarget 7, 19575–19588.
Churchill, C.D.M., Winter, P., Tuszynski, J.A., Levin, M., 2019. Electroceutical design environment: an ion channel database with small molecule modulators and tissue expression information. iScience 11, 42–56.
Djamgoz, M.B.A., 2014. Biophysics of cancer: cellular excitability “CELEX” hypothesis of metastasis. J. Clin. Exp. Oncol. S1, 005.
Durant, F., Morokuma, J., Fields, C., Williams, K., Adams, D.S., Levin, M., 2017. Long-term, stochastic editing of regenerative anatomy via targeting endogenous bioelectric gradients. Biophys. J. 112, 2231–2243.

Emmons-Bell, M., Durant, F., Hammelman, J., Bessonov, N., Volpert, V., Morokuma, J., Pinet, K., Adams, D.S., Pietak, A., Lobo, D., Levin, M., 2015. Gap junctional blockade stochastically induces different species-specific head anatomies in genetically wild-type Girardia dorotocephala flatworms. Int. J. Mol. Sci. 16, 27865–27896.

Foppen, R.J.G., van Mil, H.G.J., van Heukelom, J.S., 2002. Effects of chloride transport on bistable behaviour of the membrane potential in mouse skeletal muscle. J. Physiol. 542, 181–191.

Herrera-Rincon, C., Golding, A.S., Moran, K.M., Harrison, C., Martyniuk, C.J., Guay, J.A., Zaltsman, J., Carabello, H., Kaplan, D.L., Levin, M., 2018. Brief local application of progesterone via a wearable bioreactor induces long-term regenerative response in adult Xenopus hindlimb. Cell Rep. 25, 1593–1609.

Hille, B., 1992. Ion Channels of Excitable Membranes. Sinauer Associates, Sunderland.

Huguet, G., Joglekar, A., Messi, L.M., Buckalew, R., Wong, S., Terman, D., 2016. Neuroprotective role of gap junctions in a neuron astrocyte network model. Biophys. J. 111, 452–462.

Kamm, R.D., Bashir, R., 2014. Creating living cellular machines. Ann. Biomed. Eng. 42, 445–459.

Kamm, R.D., Bashir, R., Arora, N., Dar, R.D., Gillette, M.U., Griffith, L.G., Kemp, M.L., Kinlaw, K., Levin, M., Martin, A.C., McDevitt, T.C., Nerem, R.M., Powers, M.J., Saif, T.A., Sharpe, J., Takayama, S., Takeuchi, S., Weiss, R., Ye, K., Yevick, H., Zaman, M., 2018. Perspective: the promise of multi-cellular engineered living systems. APL Bioengineering 2, 040901.

Kirkton, R.D., Bursac, N., 2011. Engineering biosynthetic excitable tissues from unexcitable cells for electrophysiological and cell therapy studies. Nat. Commun. 2, 300.

Koseska, A., Bastiaens, P.I.H., 2017. Cell signaling as a cognitive process. EMBO J. 36, 562–582.

Krüger, J., Bohrmann, J., 2015. Bioelectric patterning during oogenesis: stage-specific distribution of membrane potentials, intracellular pH and ion-transport mechanisms in Drosophila ovarian follicles. BMC Dev. Biol. 15, 1.

Law, R., Levin, M., 2015. Bioelectric memory: modeling resting potential bistability in amphibian embryos and mammalian cells. Theor. Biol. Med. Model. 12, 22.

Levin, M., 2014. Molecular bioelectricity: how endogenous voltage potentials control cell behavior and instruct pattern regulation in vivo. Mol. Biol. Cell 25, 3835–3850.

Levin, M., Pezzulo, G., Finkelstein, J.M., 2017. Endogenous bioelectric signaling networks: exploiting voltage gradients for control of growth and form. Annu. Rev. Biomed. Eng. 19, 353–387.

Lobo, D., Solano, M., Bubenik, G.A., Levin, M., 2014. A linear-encoding model explains the variability of the target morphology in regeneration. J. R. Soc. Interface 11, 20130918.

Ma, B., Buckalew, R., Du, Y., Kiyoshi, C.M., Alford, C.C., Wang, W., McTigue, D.M., Enyeart, J.J., Terman, D., Zhou, M., 2016. Gap junction coupling confers isopotentiality on astrocyte syncytium. Glia 64, 214–226.

Macía, J., Posas, F., Sole, R.V., 2012. Distributed computation: the new wave of synthetic biology devices. Trends Biotechnol. 30, 342–349.

Mathews, J., Levin, M., 2017. Gap junctional signaling in pattern regulation: physiological network connectivity instructs growth and form. Dev. Neurobiol. 77, 643–673.

McNamara, H.M., Zhang, H., Werley, C.A., Cohen, A.E., 2016. Optically controlled oscillators in an engineered bioelectric tissue. Phys. Rev. X 6, 031001.

McNamara, H.M., Dodson, S., Huang, Y.L., Miller, E.W., Sandstede, B., Cohen, A.E., 2018. Geometry-dependent arrhythmias in electrically excitable tissues. Cell Syst 7, 359–370.

Meinhardt, H., 2012. Turing's theory of morphogenesis of 1952 and the subsequent discovery of the crucial role of local self-enhancement and long-range inhibition. Interface Focus 2, 407–416.

Mehta, P., Gregor, T., 2010. Approaching the molecular origins of collective dynamics in oscillating cell populations. Curr. Opin. Genet. Dev. 20, 574–580.

Morelli, L.G., Uriu, K., Ares, S., Oates, A.C., 2012. Computational approaches to developmental patterning. Science 336, 187–191.

Musa, H., Fenn, E., Crye, M., Gemel, J., Beyer, E.C., Veenstra, R.D., 2004. Amino terminal glutamate residues confer spermine sensitivity and affect voltage gating and channel conductance of rat connexin 40 gap junctions. J. Physiol. 557, 863–878.

Mustard, J., Levin, M., 2014. Bioelectrical mechanisms for programming growth and form: taming physiological networks for Soft body Robotics. Soft Robot. 1, 169–191.

O'Leary, T., Williams, A.H., Franci, A., Marder, E., 2014. Cell types, network homeostasis, and pathological compensation from a biologically plausible ion channel expression model. Neuron 82, 809–821.

Olimpio, E.P., Dang, Y., Youk, H., 2018. Statistical dynamics of spatial-order formation by communicating cells. iScience 2, 27–40.

Pai, V.P., Lemire, J.M., Chen, Y., Lin, G., Levin, M., 2015. Local and long-range endogenous resting potential gradients antagonistically regulate apoptosis and proliferation in the embryonic CNS. Int. J. Dev. Biol. 59, 327–340.

Pai, V., Pietak, A., Willocq, V., Ye, B., Shi, N.-Q., Levin, M., 2018. HCN2 rescues brain defects by enforcing endogenous voltage pre-patterns. Nat. Commun. 9, 998.

Palacios-Prado, N., Bukauskas, F.F., 2009. Heterotypic gap junction channels as voltage-sensitive valves for intercellular signaling. Proc. Natl. Acad. Sci. U.S.A. 106, 14855–14860.

Paré, J.-F., Martyniuk, C.J., Levin, M., 2017. Bioelectric regulation of innate immune system function in regenerating and intact Xenopus laevis. NPJ Regen. Med. 2, 15.

Pezzulo, G., Levin, M., 2016. Top-down models in biology: explanation and control of complex living systems above the molecular level. J. R. Soc. Interface 13, 20160555.

Pezzulo, G., Levin, M., 2015. Re-membering the body: applications of computational neuroscience to the top-down control of regeneration of limbs and other complex organs. Integr. Biol. (Camb.) 7, 1487–1517.

Pietak, A., Levin, M., 2016. Exploring instructive physiological signaling with the bioelectric tissue simulation engine. Front. Bioeng. Biotechnol. 4, 55.

Pietak, A., Levin, M., 2017. Bioelectric gene and reaction networks: computational modelling of genetic, biochemical and bioelectrical dynamics in pattern regulation. J. R. Soc. Interface 14, 0425.

Richardson, M.K., 2009. Diffusible gradients are out –an interview with Lewis Wolpert. Int. J. Dev. Biol. 53, 659–662.

Sheldon, R.E., Mashayamombe, C., Shi, S.-Q., Garfield, R.E., Shmygol, A., Blanks, A.M., van den Berg, H.A., 2014. Alterations in gap junction connexin43/connexin 45 ratio mediate a transition from quiescence to excitation in a mathematical model of the myometrium. J. R. Soc. Interface 11, 20140726.

Shimojo, H., Kageyama, R., 2016. Making waves toward the shore by synchronicity developmental. Cell 36, 358–359.

Sin, W.-C., Crespin, S., Mesnil, M., 2012. Opposing roles of connexin43 in glioma progression. Biochim. Biophys. Acta 1818, 2058–2067.

Soto, A.M., Sonnenschein, C., 2011. The tissue organization field theory of cancer: a testable replacement for the somatic mutation theory. Bioessays 33, 332–340.

Staufer, O., Weber, S., Bengtson, C.P., Bading, H., Rustom, A., Spatz, J.P., 2019. Adhesion Stabilized en Masse Intracellular Electrical Recordings from Multicellular Assemblies. Nano Lett. https://doi.org/10.1021/acs.nanolett.9b00784.

Sundelacruz, S., Levin, M., Kaplan, D.L., 2009. Role of membrane potential in the regulation of cell proliferation and differentiation. Stem Cell Rev. Rep. 5, 231–246.

Tong, J.J., Liu, X., Dong, L., Ebihara, L., 2004. Exchange of gating properties between rat Cx46 and chicken Cx45.6. Biophys. J. 87, 2397–2406.

Tsiairis, C.D., Aulehla, A., 2016. Self-Organization of embryonic genetic oscillators into spatiotemporal wave patterns. Cell 164, 656–667.

Tuszynski, J., Tilli, T.M., Levin, M., 2017. ion channel and neurotransmitter modulators as electroceutical approaches to the control of cancer. Curr. Pharmaceut. Des. 23, 4827–4841.

van Mil, H., van Heukelomb, J.S., Bier, M., 2003. A bistable membrane potential at low extracellular potassium concentration. Biophys. Chem. 106, 15–21.

Vandenberg, L.N., Adams, D.S., Levin, M., 2012. Normalized shape and location of perturbed craniofacial structures in the Xenopus tadpole reveal an innate ability to achieve correct morphology. Dev. Dynam. 241, 863–878.

Verdia-Baguena, C., Queralt-Martin, M., Aguilella, V.M., Alcaraz, A., 2012. Protein ion channels as molecular ratchets. Switchable current modulation in outer membrane protein F porin induced by millimolar La^{3+} ions. J. Phys. Chem. C 116, 6537–6542.

Yang, M., Brackenbury, W.J., 2013. Membrane potential and cancer progression. Front. Physiol. 4, 185.

Zhang, Y., Levin, M., 2009. Particle tracking model of electrophoretic morphogen movement reveals stochastic dynamics of embryonic gradient. Dev. Dynam. 238, 1923–1935.